Offshore AC Fault Protection of Diode Rectifier Unit Based HVDC System for Wind Energy Transmission

Rui Li, Lujie Yu, and Lie Xu, *Senior Member, IEEE*

***Abstract*—A decentralized control strategy with fast fault current providing capability and negative current control function is proposed to ride-through offshore AC faults for wind turbines (WTs) connecting with diode rectifier unit based HVDC system. A voltage-error-dependent fault current injection is proposed to regulate the WT current during fault transients and quickly provide fault current. The current controller developed in double synchronous reference frame can effectively regulate the negative currents to ensure continuous operation of WTs without overcurrent during symmetric or asymmetrical faults. A simple and effective offshore AC fault protection solution, combining both overcurrent protection and differential protection, is proposed by utilizing the developed fast fault current providing control. The proposed scheme is robust to offshore AC faults and can automatically restore normal operation. Simulation results confirms the proposed fault protection strategy.**

***Index Terms*— diode rectifier unit based HVDC (DRU-HVDC), fault protection, HVDC transmission, negative-sequence current control, offshore wind farm.**

I. Introduction

With the fast development of the high voltage DC (HVDC) technology based on voltage-source-converters (VSCs), offshore wind power will play an important role in the Europe electricity market in the near future [1-3]. To reduce the cost related to offshore wind power integration, the diode rectifier based HVDC (DR-HVDC) has recently received notable interests [4-10]. By replacing the VSC offshore station with diode rectifier, the transmission loss and the total cost can be potentially reduced by up to 20% and 30% respectively while the transmission capacity can be increased by a third [5, 11]. In addition, the volume and weight of the platform are reduced by 80% and two thirds respectively. It also has the advantages of high reliability, modular design, full encapsulation, and less operation and maintenance cost, etc. [5, 11].

Reference [4] presents a voltage and frequency control of the offshore wind turbines (WTs) connected with DR-HVDC system and proves that such solution is technically feasible in steady states and during transients. In [8], the developed control scheme is further tested during three-phase faults at the AC terminals of the onshore station and validates that the DR-HVDC is robust to such AC faults. However, the measurements at the point of common connection (PCC) are required for each WTs, necessitating the need for high-speed communication.

Various fault cases, including DC faults, symmetrical onshore and offshore AC faults, are investigated in [9]. However, during offshore AC fault, the AC currents of the WT converters are simply controlled at zero without considering the need for the operation of the protection relays. Reference [10] introduces an energy management scheme to regulate the input and output power of the DR-HVDC link and verifies its low voltage ride-through (LVRT) capability. However, the WTs are modelled as ideal voltage source and the interaction between the WTs and DR stations are ignored.

In [12], the *dq* reference frame is directly obtained by integrating the desired frequency (50 Hz) and thus the offshore frequency is fixed at 50 Hz during the offshore AC fault. However, the offshore wind farms (OWFs) are simplified as controllable current sources and the dynamics of the WT converters are omitted.

The paper investigates offshore AC fault protection of DR-HVDC system considering WT control and operation requirement during symmetric and asymmetric offshore AC faults. A distributed control strategy is developed where the WT converters actively provide fault current during faults to enable fault detection using both overcurrent and differential protections.

The paper is organized as follows. In Section II, the layout of the offshore wind power system with DR-HVDC is described. The distributed control strategy with fast fault current providing capability and negative current control function is proposed in Section III. In Section IV, the overcurrent and differential protections are developed to ride-through offshore AC faults. The proposed control and fault protection scheme is assessed in Section V, considering both symmetrical and asymmetrical offshore faults. Finally Section VI draws the conclusions.

II. System Configuration

The layout of the offshore wind power transmission system with DR-HVDC is illustrated in Fig. 1, which consists of three WT clusters but only Cluster 1 shows the details for simplicity. Each cluster is made up of 5 WT strings each having ten 8 MW WTs based on permanent magnet synchronous generators [13-15].

To enable encapsulation, easy transportation, and stepwise offshore platform installation, series connection of the diode rectifier units (DRUs) is adopted as shown in Fig. 1, where three DRUs are connected in series on the DC side to boost DC voltage while the AC sides are parallel connected to the wind farm clusters [11, 16]. Each DRU is made up of two series connected 12-pulse bridges with star-star-delta three-winding transformers on AC side. Filters are connected on the AC side

This project has received funding from the European Union's Horizon 2020 research and innovation programme under grant agreement No 691714.
The authors are with the Department of Electronic and Electrical Engineering, University of Strathclyde, Glasgow, G1 1XW UK (e-mail: rui.li@strath.ac.uk, lujie.yu@strath.ac.uk, lie.xu@strath.ac.uk).

of each DRU for reactive power compensation and harmonic suppression.

The hybrid modular multilevel converter (MMC) with mixed half-bridge (HB) and full-bridge (FB) submodules (SMs) in each arm is adopted for the onshore station, which regulates the DC voltage and allows reduced DC voltage operation of the DRU-HVDC link in the event of disconnecting one DRU, which will be demonstrated in Section V [17].

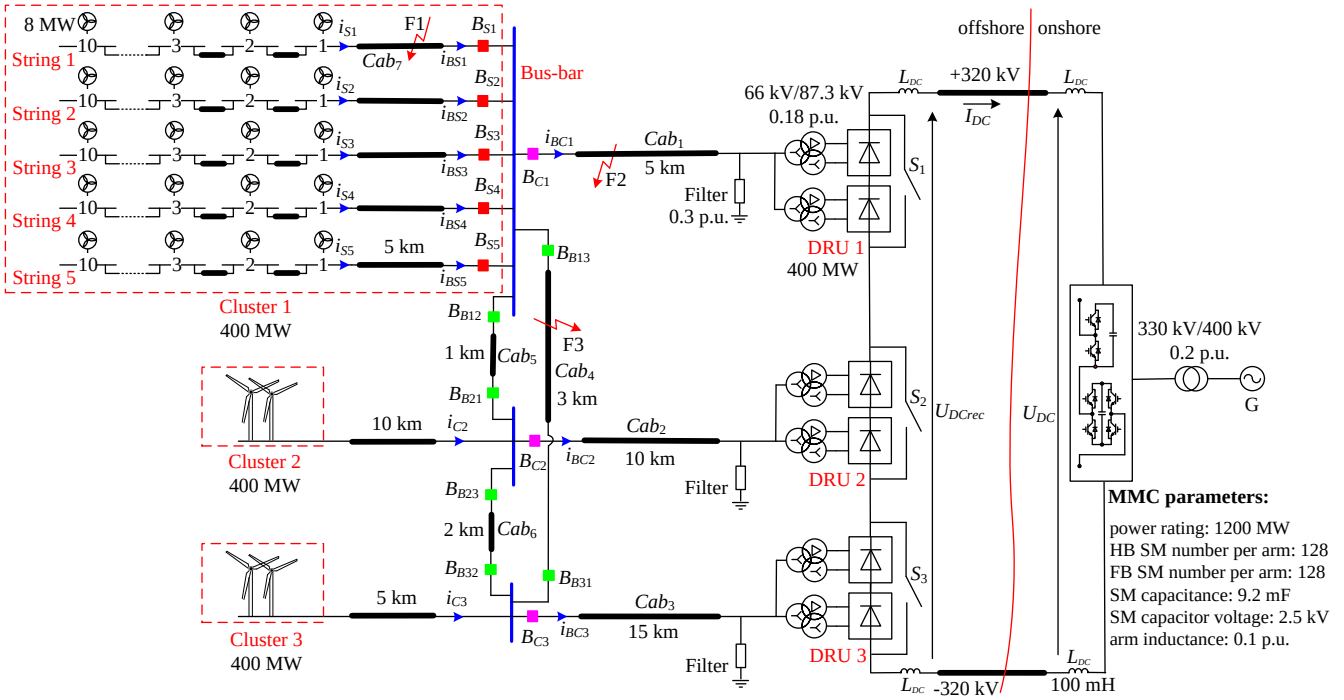

Fig. 1. Layout of the offshore wind power system with DRU-HVDC.

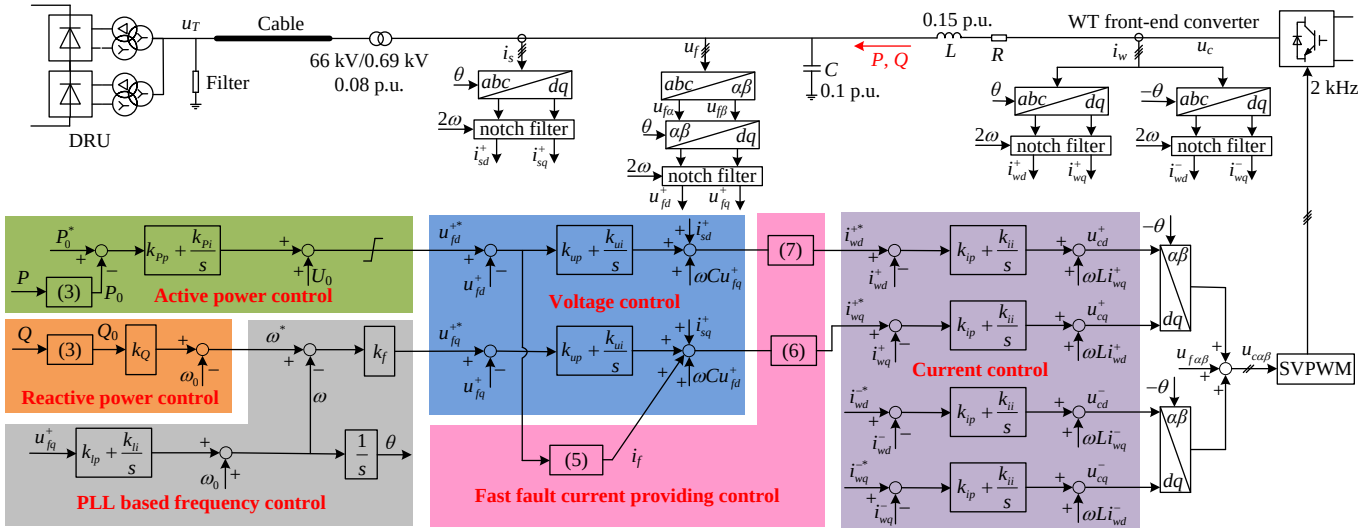

Fig. 2. Proposed control strategy of offshore WT front-end converters connected with DRU-HVDC.

III. Distributed Control Strategy of Offshore WT Front End Converters

In DRU connected OWFs, the WT generator side converters operate on DC voltage control mode while the front-end converters (FECs) control the offshore AC voltage and frequency, as well as the generated power of WTs [4, 8]. The distributed control strategy of the FECs as shown in Fig. 2 is proposed in this section, including the current loop, AC voltage magnitude and frequency control, and active and reactive power control. In order to regulate the FECs' current during offshore AC faults including asymmetrical fault, both positive and negative sequence currents have to be controlled.

A. Current Control

The current controller is developed in double synchronous reference frame to effectively suppress the negative currents during asymmetrical offshore AC faults. In positive and negative reference frames, the dynamics of the current loops are given by

$$\begin{bmatrix} u_{cd}^{+} \\ u_{cq}^{+} \end{bmatrix} = \begin{bmatrix} u_{fd}^{+} \\ u_{fq}^{+} \end{bmatrix} + L\frac{d}{dt}\begin{bmatrix} i_{wd}^{+} \\ i_{wq}^{+} \end{bmatrix} + R\begin{bmatrix} i_{wd}^{+} \\ i_{wq}^{+} \end{bmatrix} + L\begin{bmatrix} 0 & -\omega \\ \omega & 0 \end{bmatrix}\begin{bmatrix} i_{wd}^{+} \\ i_{wq}^{+} \end{bmatrix} \quad (1)$$

$$\begin{bmatrix} u_{cd}^{-} \\ u_{cq}^{-} \end{bmatrix} = \begin{bmatrix} u_{fd}^{-} \\ u_{fq}^{-} \end{bmatrix} + L\frac{d}{dt}\begin{bmatrix} i_{wd}^{-} \\ i_{wq}^{-} \end{bmatrix} + R\begin{bmatrix} i_{wd}^{-} \\ i_{wq}^{-} \end{bmatrix} + L\begin{bmatrix} 0 & -\omega \\ \omega & 0 \end{bmatrix}\begin{bmatrix} i_{wd}^{-} \\ i_{wq}^{-} \end{bmatrix} \quad (2)$$

where the superscripts '+' and '-' donate the positive and negative components in positive and negative *dq* reference frames, respectively. Notch filters as shown in Fig. 2 are used to remove the second-order components and the transfer function is:

$$G(s) = \frac{s^2 + 4\omega^2}{s^2 + 4\zeta\omega s + 4\omega^2} \quad (3)$$

where s is the Laplace operator; ω is the offshore grid angular velocity; ζ is the damping ratio.

The positive and negative sequence current controllers implemented in the positive and negative *dq* frames are used [2] and the structure is shown in Fig. 2.

The positive current references i_{wd}^{+*} and i_{wq}^{+*} are set by the offshore AC control loop, as will be presented in next subsection. With the negative current references i_{wd}^{-*} and i_{wq}^{-*} simply set at zero, the WT currents are largely balanced during an asymmetrical offshore fault, which avoids converter overcurrent and WTs can remain operational to actively provide fault current to enable fault detection and protection

B. Fast Fault Current Providing Control

To enable fault detection for protection relays, the WT converters need to remain operational and provide fast fault current response during faults. Considering the most severe fault case, where the offshore voltage largely drops to zero, the WT converters are unable to transmit active power to the DRU-HVDC link. Thus the *d*-axis current needs to reduce while the *q*-axis current is required to quickly increase to provide fault current to the offshore network. An additional component i_f is thus added to the output of the *q*-axis voltage loop to increase the *q*-axis current, as shown in Fig. 2 and (4):

$$i_{wq}^{+*} = k_{up}\left(u_{fq}^{+*} - u_{fq}^{+}\right) + k_{ui}\int\left(u_{fq}^{+*} - u_{fq}^{+}\right)dt + i_{sq}^{+} + \omega C u_{fd}^{+} + i_f . \quad (4)$$

The profile of the voltage-error-dependent fault current i_f is defined as (5) and illustrated in Fig. 3:

$$i_{f=}\begin{cases} 0, & \left(u_{fd}^{+*} - u_{fd}^{+}\right) \le U_{error1} \\ \dfrac{I_{\max}}{U_{error2} - U_{error1}}\left[\left(u_{fd}^{+*} - u_{fd}^{+}\right) - U_{error1}\right], & U_{error1} < \left(u_{fd}^{+*} - u_{fd}^{+}\right) \le U_{error2} \\ I_{\max}, & U_{error2} < \left(u_{fd}^{+*} - u_{fd}^{+}\right) \end{cases} . \quad (5)$$

During normal operation, the *d*-axis voltage u_{fq}^{+} follows the reference u_{fq}^{+*} and the voltage error $u_{fq}^{+*} - u_{fq}^{+}$ is around zero, leading to zero fault current (i_f=0). During the fault, the *d*-axis voltage loop saturates and the voltage error increases. Once $u_{fd}^{+*} - u_{fd}^{+}$ is over the lower threshold U_{error1}, i_f starts to increase. The WT converters provide maximum current (i_f=$I_{\max}$) after the voltage error becoming greater than the upper threshold U_{error2}. After fault isolation, the offshore network voltage restores and thus i_f gradually reduces. In this paper U_{error1} and U_{error2} are set at 0.5 p.u. and 0.8 p.u. respectively.

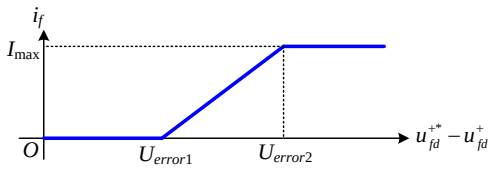

Fig. 3. Voltage-error-dependent fault current profile.

To ensure the WT converter current does not exceed its maximum value, and considering the need for the converter to provide the *q*-axis fault current, the current limits for the *d*-axis current need to be set dynamically. The upper and lower limits for the *d* and *q*-axis currents are set as:

$$i_{wqUpper}^{+*} = k_o I_{rated}, \qquad i_{wqLower}^{+*} = -k_o I_{rated} \quad (6)$$

$$i_{wdUpper}^{+*} = \sqrt{\left(k_o I_{rated}\right)^2 - \left(i_{wq}^{+*}\right)^2}, \qquad i_{wdLower}^{+*} = 0 \quad (7)$$

where k_o defines the over-load capability of the converters and is set at 1.3 in this paper. As the active power can only flow from WTs to the offshore network, the lower limit of the positive *d*-axis current $i_{wdLower}^{+*}$ is set at zero in (7) in order to avoid active power circulation among WT converters. Thus, with the increase of i_{wq}^{+*}, the *d*-axis current reference i_{wd}^{+*} reduces according to the dynamic limit depicted by (7) to avoid converter overcurrent.

C. Voltage Control

The offshore AC voltage magnitude needs to be properly regulated. Considering asymmetrical faults, the negative currents are controlled to zero. This means that only positive voltage can be actively controlled whereas the negative sequence voltage is determined by the fault impedance. The dynamics of the positive sequence voltage loops are given by

$$\begin{bmatrix} i_{wd}^{+} \\ i_{wq}^{+} \end{bmatrix} = \begin{bmatrix} i_{sd}^{+} \\ i_{sq}^{+} \end{bmatrix} + C\frac{d}{dt}\begin{bmatrix} u_{fd}^{+} \\ u_{fq}^{+} \end{bmatrix} + C\begin{bmatrix} 0 & -\omega \\ \omega & 0 \end{bmatrix}\begin{bmatrix} u_{fd}^{+} \\ u_{fq}^{+} \end{bmatrix}. \quad (8)$$

The voltage control loop sets the current references and may saturate during faults. Under such conditions, the WT converters operate on current limiting mode to provide fault current.

D. Active Power Control

During normal operation, the onshore MMC station controls its DC terminal voltage at the rated value U_{DC} and the DC current, thereby the transmitted active power, is determined by the DC terminal voltage of the DRU station U_{DCrec}:

$$I_{DC} = \frac{U_{DCrec} - U_{DC}}{R_{DC}} \quad (9)$$

where R_{DC} is the equivalent resistance of the HVDC cable. The total DC voltage produced by the DRUs U_{DCrec} is expresses as:

$$U_{DCrec} = 4 \times m \times n \times \left(\frac{3\sqrt{2}}{\pi}U_T - \frac{3}{\pi}X_T I_{DC}\right) \quad (10)$$

where U_T is the phase-to-phase voltage amplitude at the grid side of the DRU transformer; X_T is the transformer leakage reactance; n is the transformer ratio; m is the series-connected DRU number and is 3 in this paper. Then the active power of the offshore station P_{DCrec} is derived as

$$P_{DCrec} = U_{DCrec} I_{DC} = \frac{(U_{DCrec})^2 - U_{DC} U_{DCrec}}{R_{DC}} \quad (11)$$

where the DC voltage of the diode station is given as:

$$U_{DCrec} = \frac{\frac{3\sqrt{2}}{\pi} U_T + \frac{3X_T U_{DC}}{\pi R_{DC}}}{\frac{1}{4mn} + \frac{3X_T}{\pi R_{DC}}}. \quad (12)$$

As only the positive voltage is controlled and the voltage vector is aligned on the *d*-axis by the phase locked loop (PLL), the positive *d*-axis voltage u_{fd}^{+} is used to regulate the active power transferred to the DRU-HVDC link and its reference u_{fd}^{+*} is thus set by the active power controller as:

$$u_{fd}^{+*} = U_0 + k_{Pp}\left(P_0^* - P_0\right) + k_{Pi}\int\left(P_0^* - P\right)dt \quad (13)$$

where U_0 is the start-up voltage and set at 0.8 p.u. to build up the offshore AC voltage while avoid the conduction of the DRU. The *d*-axis voltage reference is in the range of 0.8-1.1 p.u. During fault, the active power loop may saturate and the offshore voltage amplitude reference is limited at 1.1 p.u.

E. Offshore Frequency and Reactive Power Control

As shown in Fig. 2, the reactive power frequency droop is adopted to share reactive power among WT converters and set the frequency reference ω^* [4, 5, 18, 19]:

$$\omega^* = \omega_0 + k_Q Q_0 \quad (14)$$

where ω_0 is the rated frequency of the offshore network.

The frequency loop considers the operating principle of the PLL, which measures the *q*-axis voltage u_{fq}^{+} and drives the offshore frequency ω to obtain zero u_{fq}^{+}, as depicted by Fig. 2 and (15):

$$\omega = \omega_0 + k_{Ip} u_{fq}^{+} + k_{Ii}\int u_{fq}^{+} dt. \quad (15)$$

The *q*-axis voltage reference u_{fq}^{+*} is set by the frequency loop and feeds to the AC voltage loop to regulate the offshore AC frequency:

$$u_{fq}^{+*} = k_f\left(\omega^* - \omega\right). \quad (16)$$

With the PLL based frequency control, the offshore frequency ω follows the reference ($\omega = \omega^*$) while the *q*-axis voltage u_{fq}^{+} is well regulated at zero [20, 21].

All the WT FECs uniformly adopt the developed control scheme, where only the local measurements are required, and can automatically ride-through the fault, as will be presented in Section V.

IV. Offshore AC Fault Protection

Due to the use of DRUs at offshore and the limited fault current providing capability of WT converters, design of offshore AC protection might have to be significantly different to that for offshore wind farms connected by either AC or VSC HVDC station.

A. Layout of Protection Relays

To examine the coordination of the WT control (providing fault currents) and the protection relays, a simplified layout of the protection relays and their connection to the DRU system is shown in Fig. 1. The main protection can be divided into the following three categories:

- **WT string**: Each string is connected to the cluster bus-bar through circuit breaker B_{Sj} (j=1, 2, …, 5) to isolate the faulty string from the AC network and ensure adequate system recovery for the healthy network. For example, the fault case F1 occurred in String 1 should lead to the opening of breaker B_{S1} to isolate the faulty String 1 from the rest of the network.
- **Cluster interconnection**: The three clusters are interconnected together through three AC cables (Cab_4, Cab_5, and Cab_6) with each end equipped with breakers to isolate the fault (F3, Fig. 1) at the ring cluster interconnection cables.
- **WT cluster**: Breaker B_{Cj} (j=1, 2, 3) is equipped at one end of the cluster cable (Cab_1, Cab_2, and Cab_3, Fig. 1) near the cluster bus-bar to isolate the fault (F2, Fig. 1) occurred at cluster cables from the wind farm.

  Considering the fault (F2, Fig. 1) applied at Cab_1, breaker B_{C1} opens to disconnect Cab_1 and then the wind power of Cluster 1 can be transmitted to onshore by the DRUs 2 and 3 through the ring cluster interconnection cables. To enable such power transfer, the DRU-HVDC link is operated with reduced DC voltage ($⅔U_{DC}$) regulated by the onshore hybrid MMC station. The DRU connected with the faulty branch (DRU 1, Fig. 1) is bypassed by the DC switch (S_1, Fig. 1) to reduce the conduction losses resulting from the power flow through the faulty DRU.

  After the reduction of the DC voltage, the maximum power transmission capability of the DRU-HVDC system is reduced to 0.67 p.u. To ensure DC current does not exceed the maximum value, the onshore MMC sets a maximum DC current order and if the current exceeds the maximum value, the DC voltage will increase slightly so as to automatically limit the power transmitted from the WTs [22]. In the meantime, the WTs will limit the generated power through pitch control.

  After the disconnection of the cluster cable, this arrangement is able to transmit certain wind power through the healthy parts and thus the system availability is improved.

B. Overcurrent Protection for Symmetrical Fault

1) String fault:

Although wind turbine FECs have limited fault current capability (e.g. maximum 1.3 p.u.), during a fault on one of the turbine strings, substantial overcurrent will still be present as all the other turbines will feed fault current to the faulty string.

Considering fault case F1 applied at string cable Cab_7 as shown in Fig. 1, in addition to Clusters 2 and 3, other healthy Strings 2, 3, 4, and 5 provide fault currents for breaker B_{S1}, as the FECs of all the WTs operate on current limiting mode during the fault:

$$i_{BS1} = -i_{C2} - i_{C3} - \sum_{j=2}^{5} i_{Sj}. \quad (17)$$

The current flowing through B_{S1} reverses after the fault and

is much higher than the nominal current. Thus, overcurrent protection can be adopted to open B_{S1} and isolate the fault. The breakers on the healthy strings (B_{S2}-B_{S5}) do not experience overcurrent and thus remain closed:

$$i_{BSj} = i_{Sj}, \qquad j = 2, 3, 4, 5. \tag{18}$$

The currents flowing through cluster breakers (B_{C1}-B_{C3}) reduce to around zero after the solid symmetrical fault and B_{C1}-B_{C3} also remain closed.

2) Cluster fault:

Considering fault case F2 applied at the cluster cable Cab_1 as illustrated in Fig. 1, the circuit breakers on strings (B_{S1}-B_{S5}) do not suffer any overcurrent due to the current limit capability of the wind turbine FECs:

$$i_{BSj} = i_{Sj}, \qquad j = 1, 2, ..., 5. \tag{19}$$

However, as expressed by (20), breaker B_{C1} on the faulty cluster cable experiences overcurrent provided by the three clusters and can be opened by overcurrent protection mechanism:

$$i_{BC1} = i_{C2} + i_{C3} + \sum_{j=1}^{5} i_{Sj}. \tag{20}$$

Due to the unidirectional characteristics of DRUs, the currents flowing through breakers on healthy cables (B_{C2} and B_{C3}) are reduced to around zero during the fault and thus they remain closed. The system is then operated with reduced DC voltage ($⅔U_{DC}$) as previously discussed.

By measuring overcurrent and properly setting the thresholds, the faulty string or cluster can be accurately located and the corresponding circuit breaker is selectively opened to isolate the fault. Overcurrent protection provides a relatively simple and reliable approach for the OWFs.

The ring arrangement of cables Cab_4, Cab_5, and Cab_6 provides multiple power transmission paths and reduces the potential wind energy loss during the aforementioned cluster faults. In addition, the interconnection of the clusters ensures almost identical voltages at the DRU AC terminals, leading to DC voltage sharing among the DRUs. As the same DC current flows through the series connected DRUs, the active power is also shared. The ring connection of the clusters improves the system reliability and its fault protection will be considered in the following Subsection D.

C. Overcurrent Protection for Asymmetrical Fault

The cluster cable fault F2 is considered in this subsection to demonstrate the overcurrent protection for asymmetrical faults. During an asymmetrical fault, the output current of the wind farm is distributed among the cluster breakers:

$$i_{BC1} = i_{C2} + i_{C3} + \sum_{j=1}^{5} i_{Sj} - i_{BC2} - i_{BC3}. \tag{21}$$

- **Current in the faulty phase of cluster breaker**: For the faulty phase, the wind farm currents partially flow to the DRU stations through the cluster breakers while the dominant part feeds to the fault. The currents mainly flow through the breaker B_{C1} on the faulty cluster and thus B_{C1} experiences overcurrent and can be opened.
- **Current in the healthy phase of cluster breaker**: The wind farm currents of the healthy phase are still largely shared among the cluster breakers B_{Cj} (j=1, 2, 3) and flow to the DRU station.
- **String breaker currents**: As the proposed control can effectively suppress the negative currents during asymmetrical faults, the currents flowing through the string breakers B_{S1}-B_{S5} are largely balanced and can still be expressed by (19). Thus, B_{S1}-B_{S5} do not experience overcurrent during cluster cable fault F2 and remain closed.

During an asymmetrical fault, the current of the faulty phase has similar behaviors as that during symmetrical fault while the current of the healthy phase still largely flows to the DRU station. Thus, the circuit breaker on the faulty cable detects overcurrent on the fault phase and can activate accordingly.

D. Differential Protection for Offshore Fault at Cluster Interconnection Cable

During normal operation, the currents flowing through the interconnection cables (Cab_4, Cab_5, and Cab_6) depend on the power differences among the three clusters and the AC cable impedances, and thus are usually low. During a fault (F3, Fig. 1) at the cluster interconnection cable, the power of the three clusters flows to the fault through the ring connection of cables Cab_4, Cab_5, and Cab_6, which experience large fault currents. Differential protection scheme is thus adopted for the ring connection of cables Cab_4, Cab_5, and Cab_6, where the currents flowing into and out of the cables are compared and a fault is detected if the current is out of the protection range.

During the fault at cluster interconnection cable, the string breakers (B_{S1}-B_{S5}) and the cluster breakers (B_{C1}-B_{C3}) do not experience overcurrent due the current limiting capability of WTs and the unidirectional characteristics of DRUs and thus remain closed. After the fault (F3) is isolated by circuit breakers (B_{B13} and B_{B31}), wind power transmission resumes.

The offshore AC cables have higher distributed capacitance. Thus, the protection range needs to be properly set to avoid mal-operation of differential protection under external fault [23, 24].

V. Simulation

The proposed control and protection scheme is assessed using the model shown in Fig. 1 in PSCAD X4. The parameters of the WT FECs are depicted in Fig. 2 while the generator-side converter is simplified as a DC voltage source [4, 8]. To test the system performances during an offshore AC fault at a string, the fault string (String 1, Fig. 1) is represented by a lumped converter of 80 MW (Converter 1) while the other healthy strings in Cluster 1 (Strings 2-5) and Clusters 2 and 3 are modelled as lumped converters rated at 320 MW, 400 MW, and 400 MW (Converters 2, 3, and 4), respectively. The onshore hybrid MMC station is represented by detailed submodule-based switching function model [25].

A. Performance Evaluation of the Proposed Control Strategy

1) Symmetrical Fault at String Cable

To test the proposed controller during an offshore AC fault and after fault isolation, a symmetrical solid fault F1 is applied at the string cable Cab_7 at t=0.3 s and is isolated by breaker B_{S1} at t=0.55 s.

As shown in Fig. 4 (a), the offshore AC voltage collapses

after the fault. For each converter, the *q*-axis current i_{wq}^{+} is quickly increased according to (5) to actively provide fault current whereas the *d*-axis current i_{wd}^{+} reduces to avoid converter overcurrent damage, as displayed in Fig. 4 (b), (e), and (i).

After the fault initiation, the active power control loop saturates and sets the offshore voltage reference u_{fd}^{+*} at 1.1 p.u., as shown in Fig. 4 (c) and (d). The *d*-axis voltage control loop also saturates during the fault and the converters operate on current limiting mode. After the fault is isolated by B_{S1} at t=0.55 s, the offshore voltage is gradually restored, as seen from Fig. 4 (a) and (d). Following the fault isolation and the offshore voltage restoration, the active power transmission gradually resumes, Fig. 4 (c) and (j).

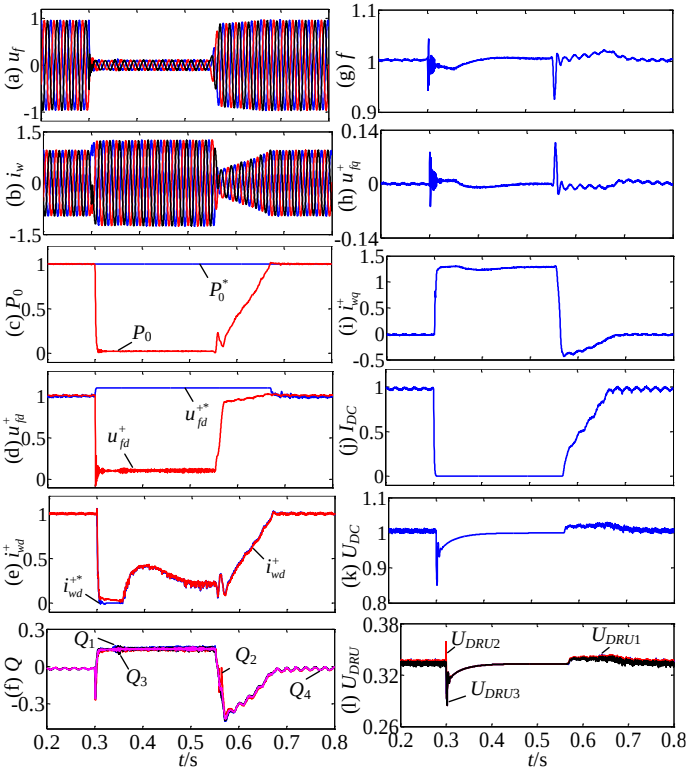

Fig. 4. Simulation results during symmetrical fault F1: (a) three-phase voltages, (b) three-phase currents, (c) active power, (d) *d*-axis voltage, (e) *d*-axis current, (f) reactive power, (g) frequency, (h) *q*-axis voltage, (i) *q*-axis current, (j) DRU-HVDC link current, (k) DRU-HVDC link voltage, and (l) DRU voltages.

During the entire simulation scenario, the reactive power are shared among the WT converters and the offshore frequency is largely controlled around the rated value of 50 Hz, as shown in Fig. 4 (f) and (g), respectively.

The DC link voltage of the DRU-HVDC slightly drops following the fault and gradually restores, as can be seen in Fig. 4 (k). In addition, the three DRUs always share the HVDC link voltage, as displayed in Fig. 4 (l).

Fig. 4 demonstrates the WT converters automatically operate on current limiting mode during the fault and can provide fast fault current response, which enables the overcurrent and differential protection and avoids communication between the WTs and the offshore protection relays, as will be discussed in Section V.B.

2) Asymmetrical Fault at String Cable

In this scenario, phases *a* and *b* are short-circuited at the middle of the string cable Cab_7 (F1, Fig. 1) at t=0.3 s and breaker B_{S1} opens at t=0.55 s to isolate the fault.

Fig. 5 compares the waveforms without and with negative current controllers. As can be seen from Fig. 5, without the negative current controller, the converter loses the control of its current resulting in significant overcurrent whereas the proposed control strategy effectively regulates the positive and negative *d*- and *q*-axis currents with the negative current controlled at around zero. Thus, the proposed controller ensures the WT converters to remain operational during the fault to actively provide fault currents to enable fault detection.

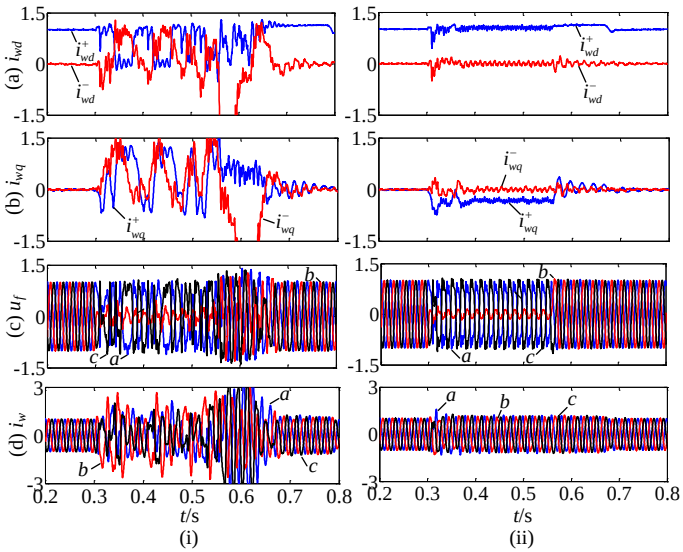

Fig. 5. Simulation results during asymmetrical fault F1 (i) without and (ii) with negative current controller: (a) positive and negative *d*-axis currents, (b) positive and negative *q*-axis currents, (c) three-phase voltages, and (d) three-phase currents.

3) Reduced DC Voltage Operation

In the event of cluster cable faults, the DRU-HVDC link is able to operate with reduced DC voltage to resume wind power transmission.

After a symmetrical fault F2 applied at the cluster cable at t=0.3 s as listed in Table I, the WT converters operate on current control mode while both the active power and *d*-axis voltage loops saturate, as aforementioned.

TABLE I
Timetable of the Reduced DC Voltage Operation.

Time	Events
0-0.3 s	Normal operation
0.3 s	Symmetrical fault occurs at cluster cable Cab_1 (F2, Fig. 1)
0.55 s	Circuit breaker B_{C1} opens
0.65-0.7 s	Onshore MMC reduces DRU-HVDC voltage

After the fault is isolated by B_{C1} at t=0.55 s, the offshore voltage gradually restores as seen from Fig. 6 (a). However as DRU 1 is disconnected from the wind farm by breaker B_{C1} with zero DC voltage output, the total DC voltage on the offshore HVDC converter side is only formed by DRUs 2 and 3 and is now lower than the onshore DC voltage controlled by the hybrid converter station. To ensure continued power transmission, the onshore hybrid MMC ramps down the DRU-

HVDC link voltage from 1 p.u. to 0.67 p.u. during (0.65-0.7 s) as displayed in Fig. 6 (i). The power transmission gradually resumes as can be seen from Fig. 6 (c). Due to the reduced DC voltage, the DC current of the DRU-HVDC link is increased from 0.6 p.u. to 0.9 p.u. to restore power transmission, Fig. 6 (j).

With the proposed control scheme, the system is robust to the cluster cable fault, where the DRU-HVDC link operates with reduced DC voltage, and the WT converters can automatically restore normal operation.

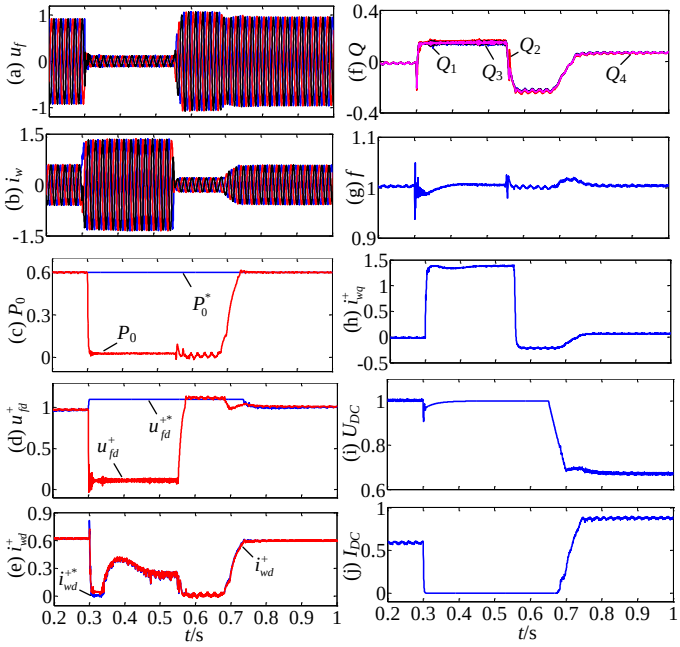

Fig. 6. Waveforms of reduced DC voltage operation during symmetrical fault F2: (a) three-phase voltages, (b) three-phase currents, (c) active power, (d) *d*-axis voltage, (e) *d*-axis current, (f) reactive power, (g) frequency, (h) *q*-axis current, (i) DRU-HVDC link voltage, and (j) DRU-HVDC link current.

B. Performance Evaluation of Proposed Protection Scheme

1) Overcurrent Protection During Symmetrical Fault

The overcurrent protection scheme is assessed during symmetrical cluster cable fault F2, as discussed in Section V A 3).

The fault currents provided by the WT converters (1.3 p.u.) feed to the fault through the circuit breaker B_{C1} and thus B_{C1} experiences overcurrent (3.9 p.u.) as shown in Fig. 7. (a), which is in agreement with (20). According to overcurrent fault detection, breaker B_{C1} is opened (assumed at t=0.55 s for illustration) without the need for communication. All other breakers do not experience overcurrent and thus remain closed, Fig. 7 (b).

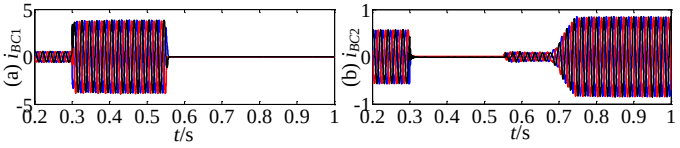

Fig. 7. Three phase currents flowing through circuit breakers during symmetrical cluster cable fault F2: (a) breaker B_{C1} on the faulty cable and (b) breaker B_{C2} on the healthy cable.

2) Overcurrent Protection During Asymmetrical Fault

An asymmetrical fault F2 occurs at the cluster cable at t=0.3 s, where phases *a* and *b* are short-circuited. As shown in Fig. 8 (a), phases *a* and *b* of breaker B_{C1} experience overcurrent and is commanded to open to isolate the fault while the breakers on the healthy cables B_{C2}, B_{C3}, and B_{S1}-B_{S5} remain closed as there is no significant overcurrent, as shown in Fig. 8 (b), (c), and (d).

3) Differential Protection During Symmetrical Fault

A symmetrical fault (F3, Fig. 1) is applied at middle of the cluster interconnection cable Cab_4 at t=0.3 s. As displayed in Fig. 9 (b), the currents flowing through the cluster breakers drop to zero after the fault (i.e. no overcurrent) and thus B_{C1}, B_{C2}, and B_{C3} remain closed.

During normal operation, the currents flowing into and out of the cable are almost identical, leading to zero current difference. As aforementioned, the WT converters quickly provide fault currents after the fault. The currents both flow into Cab_4, resulting in significant increase in the current difference, as shown in Fig. 9 (a). Once the current difference is over the protection threshold, circuit breakers B_{B13} and B_{B31} are both opened to isolate the fault and then the system automatically resumes normal operation. For illustration, B_{B13} and B_{B31} are opened at t=0.55 s in this paper.

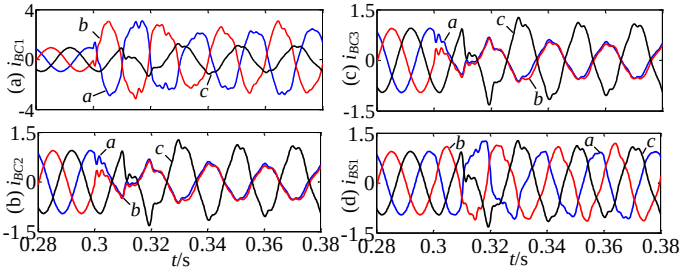

Fig. 8. Three phase currents flowing through circuit breakers during asymmetrical fault F2: (a) cluster breaker B_{C1}, (b) cluster breaker B_{C2}, (c) cluster breaker B_{C3}, and (d) string breaker B_{S1}.

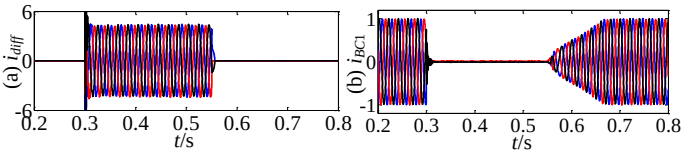

Fig. 9. Differential protection during symmetrical fault F3: (a) difference of the currents flowing into and out of cable Cab_4 and (b) currents flowing through cluster breaker B_{C1}.

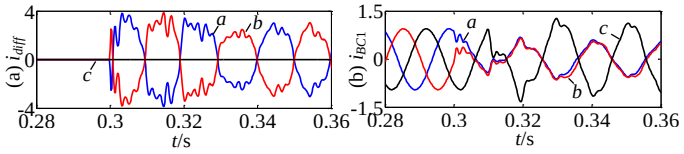

Fig. 10. Differential protection during asymmetrical fault F3: (a) difference of the currents flowing into and out of cable Cab_4 and (b) currents flowing through cluster breaker B_{C1}.

4) Differential Protection During Asymmetrical Fault

At t=0.3 s, an asymmetrical fault F3 (phases *a* and *b* shore-circuited) occurs at the cluster interconnection cable at Cab_4. For the faulty phases *a* and *b*, the differences of currents flowing into and out of cable Cab_4 significantly increase after fault as shown in Fig. 10 (a), and thus breakers B_{B13} and B_{B31} on the faulty cable are opened for fault isolation. The current differences on cluster interconnection cables Cab_5 and Cab_6 are

around zero and are not shown in Fig. 10. The cluster and string breakers do not experience overcurrent, as displayed in Fig. 10 (b).

By injecting the voltage-error-dependent fault current, the WT converters quickly provided fault currents and this enables both overcurrent protection and differential protection. In addition, the proposed protection scheme can accurately open the corresponding breaker and ensure correct operation of the protection relays.

VI. Conclusion

A decentralized control strategy is proposed to ride-through offshore AC faults for WTs connecting with DRU-HVDC system. The controller regulates the positive sequence current and suppresses the negative current to around zero during asymmetrical faults to avoid converter overcurrent. By injecting voltage-error-dependent fault currents, it enables WTs to provide fast fault current for fault detection. The proposed fault detection scheme combining overcurrent protection and differential protection can accurately activate the corresponding protection relay during various fault cases, i.e. string fault, cluster fault, and interconnection cable fault. With the proposed control and protection scheme, the WTs connecting with DRU-HVDC system can autonomously ride-through offshore AC faults and quickly resume normal operation.

VII. References

[1] E. Papatheou, N. Dervilis, A. E. Maguire, I. Antoniadou, and K. Worden, "A Performance Monitoring Approach for the Novel Lillgrund Offshore Wind Farm," *IEEE Transactions on Industrial Electronics,* vol. 62, pp. 6636-6644, 2015.

[2] L. Xu, B. R. Andersen, and P. Cartwright, "VSC transmission operating under unbalanced AC conditions - analysis and control design," *IEEE Transactions on Power Delivery,* vol. 20, pp. 427-434, 2005.

[3] A. Gandomkar, A. Parastar, and J. K. Seok, "High-Power Multilevel Step-Up DC/DC Converter for Offshore Wind Energy Systems," *IEEE Transactions on Industrial Electronics,* vol. 63, pp. 7574-7585, 2016.

[4] R. Blasco-Gimenez, S. A.-. Villalba, J. Rodríguez-D'Derlée, F. Morant, and S. Bernal-Perez, "Distributed Voltage and Frequency Control of Offshore Wind Farms Connected With a Diode-Based HVdc Link," *IEEE Transactions on Power Electronics,* vol. 25, pp. 3095-3105, 2010.

[5] S. Seman, R. Zurowski, and C. Taratoris, "Interconnection of advanced Type 4 WTGs with Diode Rectifier based HVDC solution and weak AC grids," in *Proceedings of the 14th Wind Integration Workshop,Brussels, Belgium, 20th–22nd Oct.* , 2015.

[6] C. Prignitz, H. G. Eckel, S. Achenbach, F. Augsburger, and A. Schön, "FixReF: A control strategy for offshore wind farms with different wind turbine types and diode rectifier HVDC transmission," in *2016 IEEE 7th International Symposium on Power Electronics for Distributed Generation Systems (PEDG)*, 2016, pp. 1-7.

[7] T. H. Nguyen, D. C. Lee, and C. K. Kim, "A Series-Connected Topology of a Diode Rectifier and a Voltage-Source Converter for an HVDC Transmission System," *IEEE Trans. Power Electron.,* vol. 29, pp. 1579-1584, 2014.

[8] R. Blasco-Gimenez, S. Anó-Villalba, J. Rodriguez-D'Derlée, S. Bernal-Perez, and F. Morant, "Diode-Based HVdc Link for the Connection of Large Offshore Wind Farms," *IEEE Transactions on Energy Conversion,* vol. 26, pp. 615-626, 2011.

[9] S. Bernal-Perez, S. Ano-Villalba, R. Blasco-Gimenez, and J. Rodriguez-D'Derlee, "Efficiency and Fault Ride-Through Performance of a Diode-Rectifier- and VSC-Inverter-Based HVDC Link for Offshore Wind Farms," *IEEE Transactions on Industrial Electronics,* vol. 60, pp. 2401-2409, 2013.

[10] J. Guo, D. Jiang, Y. Zhou, P. Hu, Z. Lin, and Y. Liang, "Energy storable VSC-HVDC system based on modular multilevel converter," *International Journal of Electrical Power & Energy Systems,* vol. 78, pp. 269-276, 2016/06/01/ 2016.

[11] O. Kuhn, P. Menke, R. Zurowski, T. Christ, S. Seman, G. Giering, *et al.*, "2nd generation DC grid access for offshore wind farms: HVDC in an AC fashion," *CIGRE, Paris,* pp. 1-7, 2016.

[12] M. A. Cardiel-Alvarez, J. L. Rodriguez-Amenedo, S. Arnaltes, and M. Montilla-DJesus, "Modeling and Control of LCC Rectifiers for Offshore Wind Farms Connected by HVDC Links," *IEEE Transactions on Energy Conversion,* vol. PP, pp. 1-1, 2017.

[13] R. Li and D. Xu, "Parallel Operation of Full Power Converters in Permanent-Magnet Direct-Drive Wind Power Generation System," *IEEE Transactions on Industrial Electronics,* vol. 60, pp. 1619-1629, 2013.

[14] J. Z. Zhang, T. Sun, F. Wang, J. Rodríguez, and R. Kennel, "A Computationally Efficient Quasi-Centralized DMPC for Back-to-Back Converter PMSG Wind Turbine Systems Without DC-Link Tracking Errors," *IEEE Transactions on Industrial Electronics,* vol. 63, pp. 6160-6171, 2016.

[15] L. P. Kunjumuhammed, B. C. Pal, R. Gupta, and K. J. Dyke, "Stability Analysis of a PMSG-Based Large Offshore Wind Farm Connected to a VSC-HVDC," *IEEE Transactions on Energy Conversion,* vol. 32, pp. 1166-1176, 2017.

[16] T. Kawaguchi, T. Sakazaki, T. Isobe, and R. Shimada, "Offshore-Wind-Farm Configuration Using Diode Rectifier With MERS in Current Link Topology," *IEEE Transactions on Industrial Electronics,* vol. 60, pp. 2930-2937, 2013.

[17] R. Zeng, L. Xu, L. Yao, and B. W. Williams, "Design and Operation of a Hybrid Modular Multilevel Converter," *IEEE Trans. Power Electron.,* vol. 30, pp. 1137-1146, 2015.

[18] R. Blasco-Gimenez, N. Aparicio, S. Ano-Villalba, and S. Bernal-Perez, "LCC-HVDC Connection of Offshore Wind Farms With Reduced Filter Banks," *IEEE Transactions on Industrial Electronics,* vol. 60, pp. 2372-2380, 2013.

[19] J. Renedo, A. García-Cerrada, and L. Rouco, "Reactive-Power Coordination in VSC-HVDC Multi-Terminal Systems for Transient Stability Improvement," *IEEE Transactions on Power Systems,* vol. 32, pp. 3758-3767, 2017.

[20] M. A. Zamani, A. Yazdani, and T. S. Sidhu, "A Control Strategy for Enhanced Operation of Inverter-Based Microgrids Under Transient Disturbances and Network Faults," *IEEE Transactions on Power Delivery,* vol. 27, pp. 1737-1747, 2012.

[21] H. Dong, Z. Xu, P. Song, G. Tang, Q. Xu, and L. Sun, "Optimized Power Redistribution of Offshore Wind Farms Integrated VSC-MTDC Transmissions after Onshore Converter Outage," *IEEE Transactions on Industrial Electronics,* vol. PP, pp. 1-1, 2017.

[22] R. E. Torres-Olguin, M. Molinas, and T. Undeland, "Offshore Wind Farm Grid Integration by VSC Technology With LCC-Based HVDC Transmission," *IEEE Transactions on Sustainable Energy,* vol. 3, pp. 899-907, 2012.

[23] S. Dambhare, S. A. Soman, and M. C. Chandorkar, "Adaptive Current Differential Protection Schemes for Transmission-Line Protection," *IEEE Transactions on Power Delivery,* vol. 24, pp. 1832-1841, 2009.

[24] S. Li, W. Chen, X. Yin, and D. Chen, "Protection scheme for VSC-HVDC transmission lines based on transverse differential current," *IET Generation, Transmission & Distribution,* vol. 11, pp. 2805-2813, 2017.

[25] R. Li, L. Xu, and D. Guo, "Accelerated switching function model of hybrid MMCs for HVDC system simulation," *IET Power Electronics,* 2017.